Acta Crystallographica Section A
Foundations of Crystallography
ISSN 0108-7673

Received 20 July 2011
Accepted 29 September 2011

Diffuse scattering in relaxor ferroelectrics: true three-dimensional mapping, experimental artefacts and modelling

A. Bosak,[a]* D. Chernyshov,[b] Sergey Vakhrushev[c,d] and M. Krisch[a]

[a]European Synchrotron Radiation Facility, BP 220, 38043 Grenoble Cedex, France, [b]Swiss–Norwegian Beam Lines, BP 220, 38043 Grenoble Cedex, France, [c]Ioffe Physico-Technical Institute, St Petersburg, 194021, Russian Federation, and [d]St Petersburg State Polytechnical University, Politekhnicheskaya ul. 29, St Petersburg, 195251, Russian Federation. Correspondence e-mail: bossak@esrf.fr

The available body of experimental data in terms of the relaxor-specific component of diffuse scattering is critically analysed and a collection of related models is reviewed; the sources of experimental artefacts and consequent failures of modelling efforts are enumerated. Furthermore, it is shown that the widely used concept of polar nanoregions as individual static entities is incompatible with the experimental diffuse scattering results. Based on the synchrotron diffuse scattering three-dimensional data set taken for the prototypical ferroelectric relaxor lead magnesium niobate–lead titanate (PMN–PT), a new parameterization of diffuse scattering in relaxors is presented and a simple phenomenological picture is proposed to explain the unusual properties of the relaxor behaviour. The model assumes a specific slowly changing displacement pattern, which is indirectly controlled by the low-energy acoustic phonons of the system. The model provides a qualitative but rather detailed explanation of temperature, pressure and electric-field dependence of diffuse neutron and X-ray scattering, as well as of the existence of a hierarchy in the relaxation times of these materials.

1. Introduction

Relaxor ferroelectrics have been known for more than 50 years (Smolenskii & Agranovskaya, 1958) and have attracted significant interest because of their numerous unusual properties such as the appearance of a broad peak in the real part of the dielectric permittivity as a function of temperature. This peak decreases in magnitude and shifts to higher temperature with increasing probe frequency over a very large frequency domain (Viehland *et al.*, 1990). They also have a variety of applications as sonar projectors for submarines and surface vessels as well as sensors and actuators. One of the most widely used concepts in relaxor physics is the model of polar nanoregions (PNRs), first proposed in 1973 (Burns & Scott, 1973). The starting model is based on the existence of small regions (down to a few unit cells in some directions) of local polarization, with the polarization parallel to specific high-symmetry directions. It is commonly accepted that the strong neutron and X-ray diffuse scattering in the vicinity of Bragg reflections is an experimental signature of PNRs (Xu, Shirane *et al.*, 2004), and several microscopic models have been evoked: the classical 'pancake' model (Xu, Zhong *et al.*, 2004), the generalized pancake model (Cervellino *et al.*, 2011*a*,*b*), interdomain atomic shifts (Paściak *et al.*, 2007), correlated atomic displacements (Welberry & Goossens, 2008), anisotropic strain (Vakhrushev *et al.*, 2005) or a specific type of anisotropic correlation, established *via* molecular dynamics modelling (Ganesh *et al.*, 2010). In view of numerous and longstanding contradictions between different data sets and different models, we have undertaken to analyse critically at least the most known and most cited results in this area. We have also measured the first true three-dimensional distribution of diffuse scattering in the prototypical ferroelectric relaxor – lead magnesium niobate–lead titanate (PMN–PT) – and aimed to analyse it more quantitatively than has been done previously. The paper is organized as follows: first we provide the analysis of experimental problems and possible difficulties in the data treatment, based on the previous reports and our recent data; then we analyse the existing models/parameterizations and propose a new one; finally we discuss the mechanisms underlying the new parameterization and enumerate its corollaries in the context of the available experimental observations.

2. Experiment and experimental artefacts

We have undertaken a synchrotron X-ray diffuse scattering study of lead magnesium niobate–lead titanate,

$PbMg_{1/3}Nb_{2/3}O_3$–$PbTiO_3$ (PMN–PT). The PMN–PT crystal with a Ti content of 6 at.% in the *B* sublattice was grown using a top-seeded solution growth technique (Ye *et al.*, 1990). For the measurements a needle-like fragment of ∼50 µm thickness was utilized. Its surface was etched with hot concentrated hydrochloric acid and the diffraction experiment was performed at room temperature. The diffuse scattering data set was collected at the Swiss–Norwegian Beam Lines at the ESRF with a MAR345 image-plate detector at a wavelength of 0.700 Å by rotating the sample and recording a diffraction pattern over 0.2° intervals. The experimental geometry was refined using the *CrysAlis* software (Oxford Diffraction Ltd, Abingdon, England); the resulting parameters were used for the three-dimensional reciprocal-space reconstruction. Some of the cubic symmetry elements were applied to the data in order to increase the signal-to-noise ratio. For visualization purposes the USCF *Chimera* (Pettersen *et al.*, 2005) and *POV-Ray* (http://www.povray.org) packages were used.

The diffuse scattering, observed in the proximity of Bragg reflections, is a sum of three components: (i) an intense relaxor-specific contribution (butterfly-shaped around *h*00 and ellipsoid-like around *hh*0); (ii) Huang scattering due to local distortions of the lattice; and (iii) thermal diffuse scattering (TDS) due to phonons. The specific shape of Huang scattering can be easily identified at high temperature by neutron scattering (Hiraka *et al.*, 2004; Burkovsky *et al.*, 2011), where the relaxor-specific component disappears, and the weaker TDS component remains practically hidden underneath the Huang component. Apparently, the same hierarchy of diffuse intensities is conserved in the case of X-ray scattering as well. The observed diffuse scattering in the present case is therefore dominated by the relaxor-specific contribution – the subject of the present study.

Fig. 1 accommodates the selection of experimental X-ray and neutron data for *h*00 and *hh*0 families of Bragg spots, which can be found in nearly all publications devoted to diffuse scattering in relaxors. The systems considered are: $PbMg_{1/3}Nb_{2/3}O_3$ (PMN), $PbMg_{1/3}Nb_{2/3}O_3$–$PbTiO_3$ (PMN–PT), $PbZn_{1/3}Nb_{2/3}O_3$ (PZN) and $PbMg_{1/3}Ta_{2/3}O_3$ (PMT).

Inspection of Fig. 1 leads us to conclude that while similarity between the data is found for *h*00 and *hh*0 series, independent of the system, experimental technique and sample quality, the devil is in the details. The 200 spot (Fig. 1, panel 3) displays a directional intensity minimum (corresponding to the shortest vectors *q* for a given isosurface value or to the local minima of diffuse intensity in angular space for fixed $|q|$), which is more pronounced along the *a** than along the *b** direction. This feature is hidden in panels 6 and 7 by the damaged surface layer, and can only be suspected for panels 1 and 2. Remarkably, in panel 5 the directional minimum along *b** is more pronounced than along *a**. We argue that this inversion is due to the improper choice of the integration layer thickness in reciprocal space for the Laue time-of-flight neutron diffractometer. The desired contrast variation can be mimicked when an integration layer of ±0.2 reciprocal lattice units (r.l.u.) is chosen for our experimental data (panel 4) – at variance with the thickness of *ca* ±0.005 r.l.u. (∼3 pixels in raw data) we conventionally used (panel 3). The difference for the *hh*0 series is even more pronounced. The directional minimum along the [110] direction, clearly visible in panel 10, disappears for all the other data sets (it might still be suspected in panel 13). As before, we can relate this disappearance to *Q*-resolution effects.

More generally, we note that the local minima of intensity appear in the direction roughly parallel to the momentum transfer of the corresponding Bragg node – for all the reflections. Consequently, the asymmetry of diffuse scattering for the nodes out of high-symmetry planes/directions is imposed and, obviously, observed (but was neglected in all the previous modelling attempts). An inspection of diffuse scattering near *hk*0 ($h \neq k$), where such features are discriminating and easy to detect, shall serve as an illustration: the intensity asymmetry of X-ray diffuse clouds around the 210 and 310 nodes is obvious from our Fig. 4, Fig. 2(*a*) of Cervellino *et al.* (2011*a*,*b*) and Fig. 4(*b*) of Xu, Zhong *et al.* (2004). The 210 spot is weak in neutron diffraction but some asymmetry is still seen around 310 as is evident from Fig. 5*a* of Welberry & Goossens (2008). Paściak *et al.* (2007) show experimental data only schematically with the 210 spot being symmetric – erroneously.

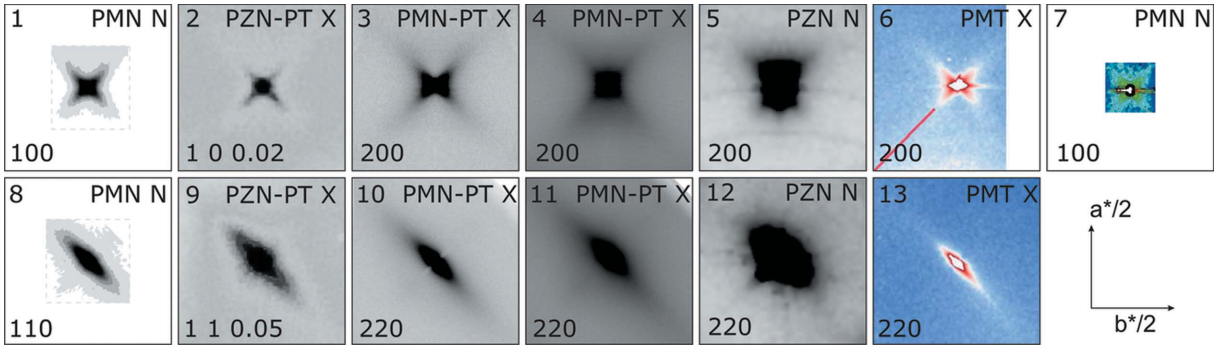

Figure 1
Comparison of the experimental data sets of various relaxors for *h*00 and *hh*0 spots. The system label (see text), *hkl* for central point and probe (X for X-rays or N for neutrons) are indicated in the individual panels. 1 and 8 refer to Hiraka *et al.* (2004); 2 and 9 refer to Xu, Zhong *et al.* (2004); 3 and 10 (integration thickness ±0.005 r.l.u.), 4 and 11 (integration thickness ±0.2 r.l.u.) refer to this work; 5 and 12 refer to Welberry (2008); 6 and 7 refer to Cervellino *et al.* (2011*a*,*b*); 7 refers to Vakhrushev *et al.* (2005).

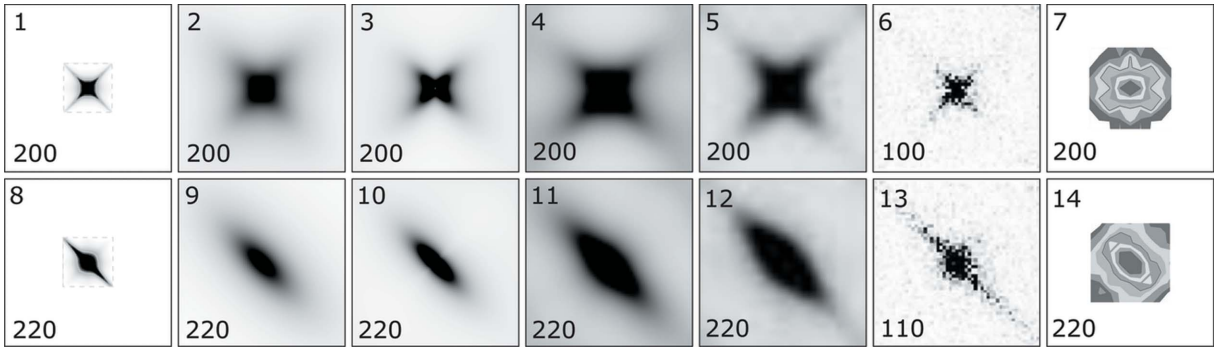

Figure 2
Comparison of the models for *h*00 and *hh*0 spots. 1 and 8 refer to Xu, Zhong *et al.* (2004); 2 and 9 refer to Cervellino *et al.* (2011*b*); 3 and 10 (no integration), 4 and 11 (integration thickness ±0.2 r.l.u.) refer to this work; 5 and 12 refer to Welberry (2008); 6 and 13 refer to Paściak *et al.* (2007); 7 and 14 refer to Ganesh *et al.* (2010). Scale and axis choice is the same as for Fig. 1; scaling of 7 and 14 is not known.

We can identify the following sources of experimental artefacts and/or misleading reduction of the experimental data:

(i) Inadequate crystalline quality. Here the majority of problems arise from surface-related scattering. Sample preparation procedures (cutting, polishing) typically produce a damaged surface layer which manifests as arcs or even powder rings superposed with Bragg reflections. These diffraction features look like streaks in the close vicinity of Bragg nodes and can be mixed up with a transverse component of diffuse scattering. For relaxors this problem was first identified in neutron scattering experiments by Vakhrushev *et al.* (2005). The issue is even more critical for X-ray scattering, where the much smaller sample sizes lead to a larger surface-to-volume ratio. Representative examples are given in Fig. 1 (panels 6, 7 and 13). Chemical etching of the sample can be considered as an appropriate solution.

(ii) Use of single images collected with an area detector. The curvature of the Ewald sphere makes any dissection of diffuse cloud curved as well; consequently a high-symmetry section of diffuse scattering distribution cannot be obtained from a single image (Fig. 1, panels 2 and 9). Series of images with a fine angular step must be taken in order to retrieve the relevant information with appropriate resolution in three orthogonal directions (see further discussion below). A detailed analysis of previously reported still images (Xu, Zhong *et al.*, 2004) is given in the supplementary materials (Fig. S1).[1] Moreover, the compensation of a misalignment of both sample and detector becomes impossible, which is not the case for the exploration of a large three-dimensional segment of the reciprocal space where corrections can be implemented *a posteriori*.

(iii) Improper choice of integration layer thickness in reciprocal space. When high-symmetry sections of reciprocal space are reconstructed, some care should be taken to keep the momentum resolution comparable in all directions. Otherwise, the excessive thickness of the integration layer results in numerous artefacts, *i.e.* a smearing or even disappearance of essential features or the emergence of new ones. This is particularly dangerous for the analysis 'by visual inspection'. The statement is applicable to the 'traditional' reconstruction using a series of images taken at varying angle (Fig. 1, panels 4 and 11, see discussion below) and to the Laue time-of-flight technique (Fig. 1, panels 5 and 12). A more detailed analysis of such artefacts is given in the supplementary materials (Fig. S2).

In the context of relaxor studies, the above-listed problems can be quite easily circumvented; the artefact-free distribution of diffuse intensity can indeed be recovered and only in this case can itserve as discriminating input for the modelling.

3. Different approaches in modelling

As can be appreciated from close inspection of the published data, the models derived on their basis could at best show an agreement for a limited set of directions/planes in reciprocal space; there is no warranty that such a modelling would not fail elsewhere or would predict features not observed experimentally. Moreover, the three-dimensional profile of diffuse clouds has never served as a criterion of model correctness despite the fact that such a comparison is more complete and therefore informative than any one-dimensional or two-dimensional profile. We are going to show that, for all lead-containing relaxors and for all the reported models, the resemblance to complete data is only approximate and sometimes vague and also further degrades when lower-symmetry spots are considered.

As an example, none of the reported models predict the local minima of intensity (see above) and the asymmetry of diffuse scattering for the nodes lying out of high-symmetry planes/directions. In fact, these features were generally overlooked and never used as an input for any model. The models yield a symmetric shape, as can be seen by inspecting Fig. 3(*a*) of Cervellino *et al.* (2011*b*), Fig. 7 of Xu, Zhong *et al.* (2004), Fig. 5(*a*) of Welberry & Goossens (2008), and the whole body of calculations presented by Paściak *et al.* (2007). Even the inspection of 'traditional' *h*00 and *hh*0 planes allows us to

[1] Supplementary materials are available from the IUCr electronic archives (Reference: DM5018). Services for accessing these data are described at the back of the journal.

conclude that a coherent description of the diffuse scattering patterns is lacking (Fig. 2).

In cases where the structure of the model and its numerical values are available (Xu, Zhong *et al.*, 2004; Cervellino *et al.*, 2011*b*), a direct comparison of the three-dimensional shape of diffuse clouds with the experimental data is feasible. We have chosen for comparison isosurface values to keep the spatial extent of diffuse objects within the range of *ca* ±0.1–0.2 r.l.u. As illustrated in Fig. 3, based on three-dimensional representations of equal intensity surfaces, the deficiency of available models involving polar nanoregions (Figs. 3*b*, 3*c*, 3*d*) is quite striking. When the isosurface level is changed, all inspected PNR models deviate from the experiment quite rapidly, indicating a departure from experimental q-dependence of diffuse intensity.

One more discrimination criterion, which can be applied to the most popular model of polar nanoregions, is the decay of diffuse intensity with reduced momentum transfer. The variety of PNR-related models assume quite different forms of the peak shape function, corresponding to the Fourier transform of the autocorrelation function of the PNR shape:

$$G(\mathbf{q}) = \frac{\xi_{//}}{1 + q_{//}^2 \xi_{//}^2} \frac{\xi_{\perp}}{1 + q_{\perp}^2 \xi_{\perp}^2} \tag{1}$$

$$G(\mathbf{q}) = \frac{\xi_{//}}{1 + q_{//}^2 \xi_{//}^2} \frac{\xi_{\perp}^2}{\left(1 + q_{\perp}^2 \xi_{\perp}^2\right)^{3/2}} \tag{2}$$

$$G(\mathbf{q}) = \frac{\xi_1}{1 + \left(\xi_1 \mathbf{w}_1 \mathbf{q}\right)^2} \frac{\xi_2}{1 + \left(\xi_2 \mathbf{w}_2 \mathbf{q}\right)^2} \frac{\xi_3}{1 + \left(\xi_2 \mathbf{w}_3 \mathbf{q}\right)^2} \tag{3}$$

$$G(\mathbf{q}) = \frac{\xi_1 \xi_2 \xi_3}{\left[1 + \left(\xi_1 \mathbf{w}_1 \mathbf{q}\right)^2 + \left(\xi_2 \mathbf{w}_2 \mathbf{q}\right)^2 + \left(\xi_2 \mathbf{w}_3 \mathbf{q}\right)^2\right]^2}. \tag{4}$$

Here ξ_1, ξ_2, ξ_3 correspond to the average dimensions of the polar nanoregions along the set of three orthogonal directions defined by the unit vectors $\mathbf{w}_1$, $\mathbf{w}_2$, $\mathbf{w}_3$ and are reduced to $\xi_{//}$ and $\xi_{\perp}$ for the axially symmetric regions. Equation (1), adopted from Xu, Zhong *et al.* (2004), is apparently wrong for reasons of dimensionality (which should be ξ^3 for a dimensionless autocorrelation function in three-dimensional space); its corrected version appears in the work of Cervellino *et al.* (2011*b*) [equation (2)]. The generalized pancake model [equation (3)] was proposed by Cervellino *et al.* (2011*a*) and further transformed to the anisotropic Lorentzian model in Cervellino *et al.* (2011*b*) [equation (4)], where PNRs are 'baguette'-shaped rather than 'pancakes'. All these models are internally deficient as they predict the decay of diffuse intensity varying with direction from q^{-2} to q^{-4}, q^{-5} and even q^{-6}, in contradiction with available experimental data (You, 2000; Chetverikov *et al.*, 2002; Vakhrushev *et al.*, 1989). Inspection of our data reveals, in agreement with previous experiments, that the deviation of the diffuse scattering intensity from q^{-2}-dependence is quite moderate in the low-q region and never behaves as q^{-4} (see supplementary materials, Fig. S3). Altogether, these data do not agree with any PNR of any shape and call for a new approach in the modelling of diffuse scattering in relaxors.

We first note that the observed distribution of diffuse intensity strongly resembles the pattern of thermal diffuse scattering for cubic crystals, while it is known that in the present case the diffuse scattering is essentially of (quasi)-elastic nature (Gehring *et al.*, 2009). However, close similarity of observed diffuse clouds to what one would formally expect for TDS led us to model the diffuse scattering in close analogy to the formalism for TDS (X-ray case):

$$I \propto f_{\mathrm{Pb}}^2(Q) \exp[-2W_{\mathrm{Pb}}(Q)] \times \frac{\sin^2(2\pi r_0 Q)}{Q^2} \cdot \mathbf{Q}^T \cdot \frac{\coth\{\alpha[\Sigma(\mathbf{Q})]^{1/2}\}}{[\Sigma(\mathbf{Q})]^{1/2}} \cdot \mathbf{Q}, \tag{5}$$

where Q is the momentum transfer, f_{Pb} is the atomic scattering factor of the lead ion (Cromer & Mann, 1968), W_{Pb} is the Debye–Waller factor (Zhukov *et al.*, 1995) and α is a constant that for real TDS depends on temperature. The $\sin(2\pi r_0 Q)/Q$ term describes the possible locations of the Pb ion over a shell of radius r_0 (Zhukov *et al.*, 1995), and the symmetric tensor $\Sigma(\mathbf{Q})$ is defined as

$$\Sigma_{\alpha\alpha}(\mathbf{Q}) = \Psi_{11}\{2 - \cos(2\pi Q_\alpha)[\cos(2\pi Q_\beta) + \cos(2\pi Q_\gamma)]\} + (2\Psi_{44} - \Psi_{12})[1 - \cos(2\pi Q_\beta)\cos(2\pi Q_\gamma)] \tag{6a}$$

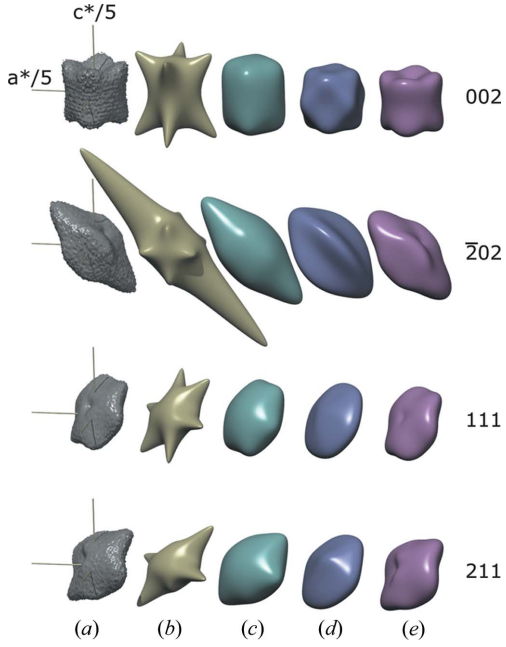

Figure 3
Comparison of (*a*) experimental (PMN–PT) and model isosurfaces of diffuse scattering intensity in the proximity of different Bragg nodes. (*b*) Denotes the axially symmetric pancake model by Xu, Zhong *et al.* (2004) with parameters given by Cervellino *et al.* (2011*b*), (*c*) refers to its modification following Cervellino *et al.* (2011*b*) with the same parameters, (*d*) corresponds to the modified pancake ('baguette') model of Cervellino *et al.* (2011*b*) and (*e*) stands for the model of the present paper. Isosurface values were chosen in order to keep the spatial extent of objects within the range of *ca* ±0.1–0.2 r.l.u.

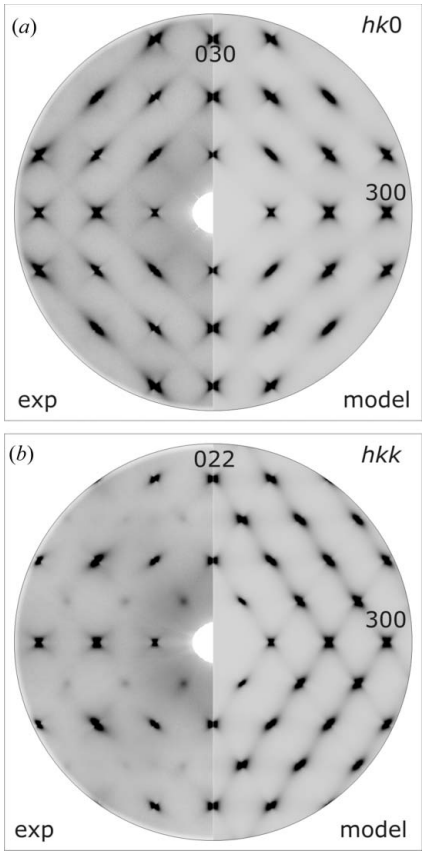

Figure 4
Experimental and model diffuse scattering intensity distribution of PMN–PT in (*a*) *hk*0 and (*b*) *hkk* planes. For the reconstruction of the experimental patterns selected symmetry elements of the crystal were applied. Diffuse spots with non-integer Miller indices visible in the *hkk* plane point towards correlated Mg/Nb disorder, where nearest neighbours tend to be of a different type, thus locally resembling the NaCl structure. Constant background is added to facilitate the comparison.

$$\Sigma_{\alpha\beta}(\mathbf{Q}) = (\Psi_{44} + \Psi_{12})\sin(2\pi Q_\alpha)\sin(2\pi Q_\beta). \qquad (6b)$$

Here $\alpha, \beta, \gamma = 1, 2, 3$, $\alpha \neq \beta \neq \gamma$. Near reciprocal-lattice nodes $\boldsymbol{\tau}$ ($\mathbf{Q} = \boldsymbol{\tau} + \mathbf{q}$) $\Sigma(\mathbf{Q})$ simplifies to $\Sigma_{jk}(\mathbf{q}) = 4\pi^2\Psi_{ijkl}q_iq_l$. Here, the tensor Ψ accommodates cubic symmetry, and consequently we obtain in Voigt notation the following equation:

$$\Sigma(\mathbf{q}) = 4\pi^2\begin{bmatrix} \Psi_{11}q_x^2 + \Psi_{44}(q_y^2+q_z^2) & (\Psi_{12}+\Psi_{44})q_xq_y & (\Psi_{12}+\Psi_{44})q_xq_z \\ (\Psi_{12}+\Psi_{44})q_xq_y & \Psi_{11}q_y^2 + \Psi_{44}(q_x^2+q_z^2) & (\Psi_{12}+\Psi_{44})q_yq_z \\ (\Psi_{12}+\Psi_{44})q_xq_z & (\Psi_{12}+\Psi_{44})q_yq & \Psi_{11}q_z^2 + \Psi_{44}(q_x^2+q_y^2) \end{bmatrix}. \qquad (7)$$

We would like to emphasize that, while these expressions closely resemble the ones for the description of TDS (Bosak & Chernyshov, 2008), here Ψ_{ij} do not have the meaning of elastic modulus, and α does not have the meaning of an inverse temperature. Besides scaling by an overall intensity factor, our model depends on only three parameters: $\Psi_{ij}\alpha^2$; moreover, in the very proximity of reciprocal-lattice nodes this number reduces to two, for example Ψ_{12}/Ψ_{11} and Ψ_{44}/Ψ_{11}. The structure of $\Sigma(\mathbf{Q})$ as given by equations (6*a*) and (6*b*) creates extra Bragg spots, corresponding to face-centring in real space. These artefacts are situated far away from the region of interest, and therefore do not affect our analysis and interpretation. In fact, our proposed description remains valid for a larger region in the proximity of nodes than a similar model mimicking the primitive cubic lattice. Taking the experimental values for W_{Pb} (Q) and r_0 = 0.286 Å (Zhukov *et al.*, 1995), and adjusting the free parameters to $\Psi_{11}\alpha^2 = 0.121$, $\Psi_{12}\alpha^2 = 0.097$ and $\Psi_{44}\alpha^2 = 0.049$, we reproduce extremely well two-dimensional (Figs. 4*a*, 4*b*) and three-dimensional diffuse scattering patterns taken at room temperature (Figs. 3*a* and 3*e*) in the proximity of Bragg reflections, both in terms of shape and relative intensities up to at least 0.1–0.15 r.l.u. It is important to note that our model, in contrast to all other previous models, reproduces the directional minimum of intensity for every diffuse cloud (see above). The proposed parameterization must fail both at very small q, where the system behaves like an elastic continuum, and for large q, where the approximation of the perovskite lattice dynamics by a factitious monoatomic lattice is too simplistic. The range of validity of the model can be extended to the small-q limit by the introduction of an additive isotropic tensor term in equations (5)–(7). Such an extension would account for the Ornstein–Zernike form $1/(q^2+\kappa^2)$ of diffuse scattering, experimentally observed at small q, with κ^{-1} being a correlation radius for a given temperature (Vakhrushev *et al.*, 1989); such a term could be proposed on a purely phenomenological basis disregarding the microscopic mechanism. In the following we concentrate on the intermediate-q range where only three or two parameters provide a perfect description – as is evident from the comparison of computed and observed scattering intensity isosurfaces shown in Fig. 3. Note that the same set of model parameters reproduces all the observed reflections nearly equally well (Fig. 4); this also allows prediction of diffuse scattering in great detail for reflections not covered by our experiment.

It is important to underline that our parameterization does not require the introduction of static polar nanoregions – objects of symmetry lower than the symmetry of the embedding crystal. It provides the best description of the experimentally observed diffuse scattering patterns using the cubic symmetry of the crystal as the only prerequisite, while reducing the number of free parameters from eight (for generalized pancake or anisotropic Lorentzian models) to only two or three. The proposed tensor description has a certain similarity with the description of polar glasses (Timonin *et al.*, 1998), though these models have essentially a different internal structure.

4. Results and discussion

As illustrated above, modern experimental facilities with bright X-ray sources and state-of-the-art two-dimensional detectors can provide invaluable information, under the condition that particular care is taken to avoid possible artefacts in the data collection and treatment. Artefact-free data are essential for any quantitative or semi-quantitative

modelling attempt. Based on the excellent agreement between experiment and model, and in the light of previous temperature-, pressure- and electric-field-dependent diffuse scattering studies on PMN–PT and related compounds, we propose the following mechanistic concept potentially underlying our phenomenological parameterization. In each unit cell the Pb ions are displaced from their 1*a* positions. The set of possible positions is very large and can be approximated by a spherical shell (Zhukov *et al.*, 1995). Under the assumption that neighbouring Pb ions do not substantially interact with each other but only *via* the BO_3 octahedral framework, they can be aligned together by a dynamical local distortion: a wave (phonon) with sufficient amplitude and proper polarization. The probability of obtaining a distortion of sufficiently large amplitude is inversely proportional to the frequency of the wave ($\sim\omega^{-2}$ for $\hbar\omega << k_{\rm B}T$), and the Pb displacement pattern remains frozen on the scale of typical phonon lifetimes, unless it is affected by another wave/phonon. Consequently, the quasi-elastic diffuse scattering would mimic, in first approximation, the TDS pattern from acoustic phonons. Its shape will not necessarily coincide with the shape of TDS as the interaction between the acoustic wave and the Pb displacement is not isotropic, but the symmetry of the underlying Ψ tensor near Bragg nodes must be the same as for the elastic tensor. It has been stated before that lattice dynamics in relaxors are influenced by an extra mechanism, giving rise to the elastic/quasi-elastic scattering (Stock *et al.*, 2006; Toulouse *et al.*, 2010); here we note that the model we propose assumes a displacement pattern that is mediated by phonons. The moderate deviation of diffuse intensity decay from q^{-2} for some directions could be an indication of the existence of attraction/repulsion poles on the Pb-locus sphere and requires further investigations.

As relaxor-specific diffuse scattering is related to *large* displacements of Pb from its average position, its intensity must be superior to Huang scattering and TDS at least when it is probed by X-ray scattering.

Further support for the validity of our model is provided by the fact that relative intensities of spots are reproduced in a satisfactory way using only a Pb-related pre-factor,

$$f_{\rm Pb}^2(Q)\exp[-2W_{\rm Pb}(Q)]\frac{\sin^2(2\pi r_0 Q)}{Q^2}$$

(Fig. 4). To account for neutron diffuse scattering where scattering factors for O and Pb are comparable, oxygen displacements may also become important (Hirota *et al.*, 2002); an extension of the model incorporating the displacement of oxygen and also of Mg/Nb atoms implies mainly the modification of the above-mentioned pre-factor in equation (5). However, such an extension would not affect strongly the local shape of the diffuse scattering since the pre-factor, irrespective of the structural motif involved in the calculation, is a slowly varying function of **Q**.

The recent demonstration by means of piezoresponse force microscopy (Kholkin *et al.*, 2011) of the presence of two effective order parameters, linked to the dynamic and static parts of polarization, is also in line with our observations. The dynamic part of the polarization can be directly related to our phonon-mediated mechanism, while the static component, corresponding to the labyrinthine structure on the 100 nm scale, can be considered as contributing to the k^{-1} parameter in the Ornstein–Zernike term at low *q*. Labyrinthine domains are not related to the polar nanoregions in their usual meaning as they have much larger lateral size.

The distribution of atomic displacements in space is therefore not static, but stationary in the sense of its power spectrum/diffraction and changes slowly in time compared to conventional lattice dynamics. This is incompatible with the model of static polar nanoregions of any shape/polarization. It is not obvious whether the Pb motion could be considered as equivalent to a very low energy, overdamped, strongly anharmonic mode. For instance, strong nonlinearity and anharmonicity of relaxors can result in the formation of intrinsic local modes with discrete breather-type character (Bussmann-Holder & Bishop, 2004).

The issue of the critical amplitude necessary for the switching of Pb distribution remains quite unclear. While it could be the result of normal phonon population, it may be again related to the nonlinearity of the system – and the mechanism of critical amplitude rising will be similar to the mechanism of 'rogue waves' creation (Chabchoub *et al.*, 2011). Though pure speculation, this description provides an explanation for the extremely long relaxation times.

The corollaries of our mechanistic model indeed can be corroborated by the following well known experimental facts. (i) The disappearance of a relaxor-specific component of diffuse scattering at high temperature (Hiraka *et al.*, 2004) can be explained by the transition of Pb displacements towards a free uncorrelated movement over the spherical shell. As a consequence, the structured diffuse scattering transforms to a smoothly changing background. (ii) The reduction of diffuse scattering due to the Pb movements under high pressure (Kreisel *et al.*, 2004) follows from the unavoidable creation of deep local minima on the spherical shell, in which the Pb ions remain frozen. (iii) Changes of the diffuse scattering in an applied electric field (Xu *et al.*, 2006) correspond to the creation of additional anisotropy in the energy relief over the displacement shell. As a result, diffuse scattering features perpendicular to the field direction should shrink, in agreement with experimental observations; moreover, further increase of the electric field results in the complete suppression of the diffuse signal (Vakhrushev *et al.*, 1998). (iv) After poling, the polarization in a switched domain fades uniformly with time (Kholkin *et al.*, 2011), contrary to the domain wall movement in conventional ferroelectrics. (v) The extremely large spread of relaxation times (Viehland *et al.*, 1990) is in line with a hierarchy of displacement patterns in space and their respective lifetimes. The dynamic nature of polar nanoregions has been suggested for temperatures above the characteristic Burns temperature (Gehring *et al.*, 2009). Our model assumes that the dynamic nature of diffuse scattering can be preserved even at low temperatures, therefore assuming timescales longer than 2 ns found in Gehring *et al.* (2009).

5. Conclusions

We have shown that incomplete or distorted data on diffuse scattering in relaxor ferroelectrics have provoked a plethora of models which do not meet physical reality. We have illustrated that the real distribution of diffuse intensity in prototype systems has a more complex shape than previously admitted. This complex shape, however, can be easily parameterized within a TDS-like model which is simpler than approaches used before and also reduces significantly the number of parameters. Despite the simplicity of our parameterization – with only two or three adjustable parameters – it provides the best description of the complex relaxor-specific diffuse scattering ever reported. Most importantly, our model points towards an intricate dynamical phenomenon, in stark contrast to the concept of static polar nanoregions – which apparently do not exist in the usual meaning as individual entities. We note that a quantitative derivation of the relevant parameters is still missing. The fact that the very complex diffuse pattern may be efficiently reduced to only three numbers should stimulate the further development of new phenomenological models capturing the essential physics of relaxors. For a complete theoretical understanding of the underlying mechanisms, appropriate molecular-dynamics simulations may become the key tool.

We are grateful to Efim Kats (Institut Laue–Langevin, Grenoble, France) and to Björn Winkler (Goethe-Universität, Frankfurt a.M., Germany) for the numerous fruitful discussions and the encouragement. This work was partially supported by the RFBR (grant No. 11-02-00687-a).

References

Bosak, A. & Chernyshov, D. (2008). *Acta Cryst.* A**64**, 598–600.
Burkovsky, R. G., Vakhrushev, S. B., Hirota, K. & Matsuura, M. (2011). arXiv: 1101.3873v1.
Burns, G. & Scott, B. A. (1973). *Solid State Commun.* **13**, 423–426.
Bussmann-Holder, A. & Bishop, A. R. (2004). *J. Phys. Condens. Matter*, **16**, L313–L320.
Cervellino, A., Gvasaliya, S. N., Zaharko, O., Roessli, B., Rotaru, G. M., Cowley, R. A., Lushnikov, S. G., Shaplygina, T. A. & Fernandez-Diaz, M.-T. (2011*a*). arXiv: 0908.2920v2.
Cervellino, A., Gvasaliya, S. N., Zaharko, O., Roessli, B., Rotaru, G. M., Cowley, R. A., Lushnikov, S. G., Shaplygina, T. A. & Fernandez-Diaz, M. T. (2011*b*). *J. Appl. Cryst.* **44**, 603–609.
Chabchoub, A., Hoffmann, N. P. & Akhmediev, N. (2011). *Phys. Rev. Lett.* **106**, 204502.
Chetverikov, Yu. O., Naberezhnov, A. A., Vakhrushev, S. B., Dorner, B. & Ivanov, A. (2002). *Appl. Phys. A*, **74**, S989–S991.
Cromer, D. T. & Mann, J. B. (1968). *Acta Cryst.* A**24**, 321–324.
Ganesh, P., Cockayne, E., Ahart, M., Cohen, R. E., Burton, B., Hemley, R. J., Ren, Y., Yang, W. & Ye, Z.-G. (2010). *Phys. Rev. B*, **81**, 144102.
Gehring, P. M., Hiraka, H., Stock, C., Lee, S.-H., Chen, W., Ye, Z.-G., Vakhrushev, S. B. & Chowdhuri, Z. (2009). *Phys. Rev. B*, **79**, 224109.
Hiraka, H., Lee, S.-H., Gehring, P. M., Xu, G. & Shirane, G. (2004). *Phys. Rev. B*, **70**, 184105.
Hirota, K., Ye, Z.-G., Wakimoto, S., Gehring, P. M. & Shirane, G. (2002). *Phys. Rev. B*, **65**, 104105.
Kholkin, A., Morozovska, A., Kiselev, D., Bdikin, I., Rodriguez, B., Wu, P., Bokov, A., Ye, Z.-G., Dkhil, B., Chen, L.-Q., Kosec, M. & Kalinin, S. V. (2011). *Adv. Funct. Mater.* **21**, 1977–1987.
Kreisel, J., Bouvier, P., Dkhil, B., Chaabane, B., Glazer, A., Thomas, P. & Welberry, T. (2004). *Ferroelectrics*, **302**, 293–298.
Paściak, M., Wołcyrz, M. & Pietraszko, A. (2007). *Phys. Rev. B*, **76**, 014117.
Pettersen, E. F., Goddard, T. D., Huang, C. C., Couch, G. S., Greenblatt, D. M., Meng, E. C. & Ferrin, T. E. (2005). *J. Comput. Chem.* **25**, 1605–1612.
Smolenskii, G. A. & Agranovskaya, A. I. (1958). *Zh. Tekh. Fiz.* **28**, 1491–1493.
Stock, C., Ellis, D., Swainson, I. P., Xu, G., Hiraka, H., Zhong, Z., Luo, H., Zhao, X., Viehland, D., Birgeneau, R. J. & Shirane, G. (2006). *Phys. Rev. B*, **73**, 064107.
Timonin, P. N., Zakharchenko, I. N., Bunina, O. A. & Sakhnenko, V. P. (1998). *Phys. Rev. B*, **58**, 3015–3021.
Toulouse, J., Iolin, E., Hennion, B., Petitgrand, D., Yong, G. & Erwi, R. (2010). arXiv: 1001.4096v2.
Vakhrushev, S., Ivanov, A. & Kulda, J. (2005). *Phys. Chem. Chem. Phys.* **7**, 2340–2345.
Vakhrushev, S. B., Kvyatkovsky, B. E., Naberezhnov, A. A., Okuneva, N. M. & Toperverg, B. P. (1989). *Physica B*, **156–157**, 90–92.
Vakhrushev, S. B., Naberezhnov, A. A., Okuneva, N. M. & Savenko, B. N. (1998). *Phys. Solid State*, **40**, 1728–1733.
Viehland, D., Jang, S. J., Cross, L. E. & Wutting, M. (1990). *J. Appl. Phys.* **68**, 2916–2921.
Welberry, T. R. (2008). *Metall. Mater. Trans. A*, **39**, 3170–3178.
Welberry, T. R. & Goossens, D. J. (2008). *Acta Cryst.* A**64**, 23–32.
Xu, G., Shirane, G., Copley, J. R. D. & Gehring, P. M. (2004). *Phys. Rev. B*, **69**, 064112.
Xu, G., Zhong, Z., Bing, Y., Ye, Z. G. & Shirane, G. (2006). *Nat. Mater.* **5**, 134–140.
Xu, G., Zhong, Z., Hiraka, H. & Shirane, G. (2004). *Phys. Rev. B*, **70**, 174109.
Ye, Z.-G., Tissot, P. & Schmid, H. (1990). *Mater. Res. Bull.* **25**, 739–748.
You, H. (2000). *J. Phys. Chem. Solids*, **61**, 215–220.
Zhukov, S. G., Chernyshev, V. V., Aslanov, L. A., Vakhrushev, S. B. & Schenk, H. (1995). *J. Appl. Cryst.* **28**, 385–391.